All Sciences Proceedings

1st International Conference on Modern and Advanced Research

July 29-31, 2023 : Konya, Turkey

All Sciences Proceedings
http://as-proceeding.com/

https://as-proceeding.com/index.php/icmar

Impact Toughness of TIG Double-Sided Arc Welded Thick Dissimilar Plates

Tanju TEKER[1*], Ahmet GÜNEŞ[2]

[1]Sivas Cumhuriyet University, Faculty of Technology, Department of Manufacturing Engineering, 58140, Sivas, Türkiye.
[2]Hasan Hüseyin Akdoğan Vocational and Technical Anatolian School, 27700, Nizip, Gaziantep, Türkiye.

[*](tanjuteker@cumhuriyet.edu.tr) Email of the corresponding author

Abstract **–** Welding is used in manufacturing in all engineering industries. In this study, thick dissimilar steels were welded using double-sided tungsten inert gas (TIG) welding. Microstructural changes of joints were detected by using optical microscope (OM), X-Ray diffraction (XRD). Impact toughness of joints were determined by notch impact test. Fracture surface morphology was evaluated by SEM. A strong metallurgical bond appeared in the welding of the thick dissimilar plates. Full penetration was achieved without additional metal and welding gap. The widening and deepening of the weld pool increased the impact performance.

Keywords – AISI 304, DUROSTAT 500, DSAW, Microstructure, Toughness.

I. INTRODUCTION

Welding gained importance in production technology with developments in application and usability. It includes various technologies and a wide variety of materials that can be welded. The reason for joining dissimilar metals is creative engineering practices such as high strength, low specific gravity, good corrosion resistance and low cost [1], [2]. Tungsten inert gas (TIG) welding is preferred in the modern industry due to its deep penetration and high travel speed. DSAW-TIG has superiority in terms of welding efficiency and penetration ability. It can be preferred for welding dissimilar metals in the welding industry [3], [4]. Austenitic steels (ASS) are preferred for industry for their excellent weldability and corrosion performance. AISI304 steel with a surface cubic center (FCC) structure demonstrates ductility at lower temperatures than ferritic steel. The cause for this distinction is the variation in the properties of the shear planes and the orientation between the BCC and FCC alloys [5], [6]. The choice of primary phase in rapid solidification of austenitic steel is determined by nucleation mechanisms between ferrite and austenite. The activation energy provides the uniform nucleation of the primary phase in the supercooled melt. The phase with the less nucleation activation energy solidifies as the primary phase [7]. Solidification of the weld metal takes place on the grains at the boundaries of the molten pool, epitaxial growth occurs. For solid nucleation, the liquid does not need to be significantly supercooled. Therefore, the solid phase at the melting limits is effective in determining the primary phase. Primary ferrite grows and nucleates on the surface of body-centered cubic ferrite grains. Primary ferrite is difficult to nucleate on a face-centered cubic grain due to the interface energy between the BCC and FCC lattices [8]. DUROSTAT500 steel grades are steels with high resistance to mechanical wear. It is used in conveyors, excavators, road machines and crushers [9]. Cui et al. reported the impact toughness of keyhole TIG welded S32101 joints. The impact energy rised with the increase in heat input and austenite volume [10].

In this study; the impact toughness of TIG double-sided arc welded thick dissimilar plates was investigated.

II. Materials and Method

AISI304 (0.08%C, 18%Cr, 8%Ni, 2.00%Mn, 1.00%Si, 0.04%S, Bal.%Fe) and DUROSTAT500 (0.30%C, 1.00%Cr, 1.10%Mn, 0.60%Si, 0.01.%S, 0.50%Mo, Bal.%Fe) steels in 10x100x100 mm dimensions were used. Weld parameters are shown in Table 1. The samples were joined using the Ge-Ka-Mak TIG device. After sanding the samples with 180-1200 mesh abrasives, they were polished with 3 µm diamond paste. AISI304 grade was electrolytically etched in 50% alcohol + 50% HNO_3 solution, 12 V and 5-8 seconds. DUROSTAT500 grade was etched in a Nital solution. The microstructure phase analysis of samples were determined using optical microscope and CuKα (λ= 1.54058 Å) wavelength Rigaku XRD instrument. Impact qualities of joints were measured by notch impact test. Fracture surface morphology was evaluated by SEM.

Table 1. Weld parameters.

No	Weld current (A)	Shielding gas rate (l/min.)	Electrode diameter (mm)	Weld speed (m/min.)
S1	410	8	3.2	0.02
S2	420	8	3.2	0.02
S3	430	8	3.2	0.02

III. Results

3.1 Macro face evoluation

The surface and cross-sectional view of the S3 joint is given in Fig. 1. A smooth crater structure was formed in the weld seams. Increasing current intensity increased penetration and weld seam widths. Different welding profiles were formed in the joints made without the use of additional metal and without opening the weld bevel. A wide temperature gradient occurred from the center under the torch to the edges of the weld pool. A broad surface tension gradient formed across the surface. Therefore, the liquid flowed from the center of the pool to the edge, forming a large weld pool. The welding arc tended towards the ferromagnetic material side during welding [11], [12].

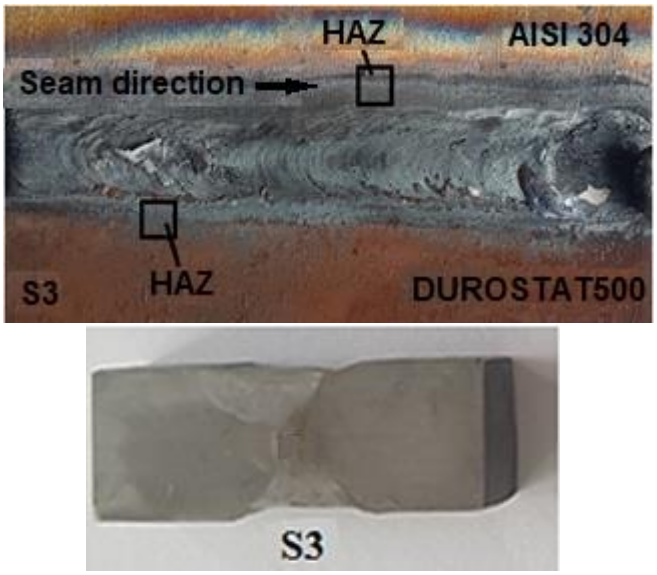

Fig. 1. Surface and cross-section view of the S3 joint.

3.2. Microstructure

Optical photo of S3 joint is displayed in Fig. 2. No weld faults were detected at the join interface. High heat input reasoned grain coarsening in near weld metal. On the HAZ-A, the grains were aligned towards the base metal in the rolling direction. Cr_7C_3 was detected at the grain boundaries. At the joints, the microstructure was divided into four parts. The melting zone is the coarse-grained zone, the fine-grained zone and the partially crystallized zone [13], [14]. On the HAZ-B, the transition zone was wider. Cementite + pearlite phases were formed in HAZ-B structure. X-Ray analysis is given in Fig. 3. The weld metal had martensite, Fe_3C, $CrFe_7C_{0.45}$, FeNi, Cr_3C_2 and Fe_3Ni_2 phases.

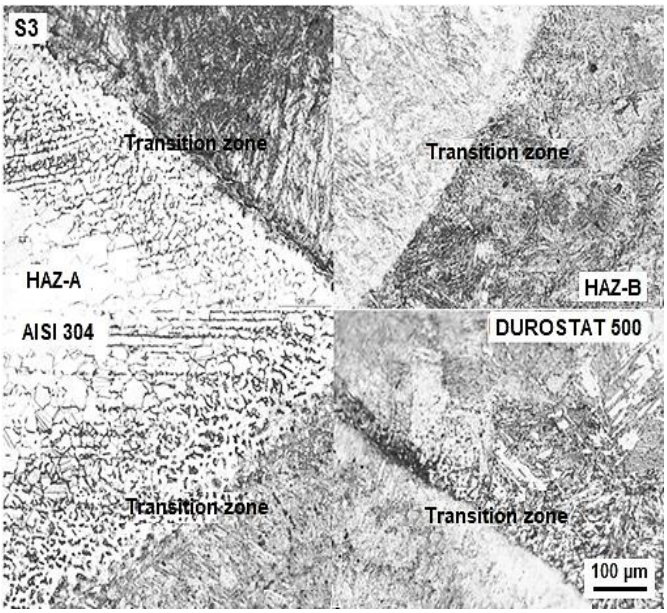

Fig. 2. Optical photograph of S3 joint.

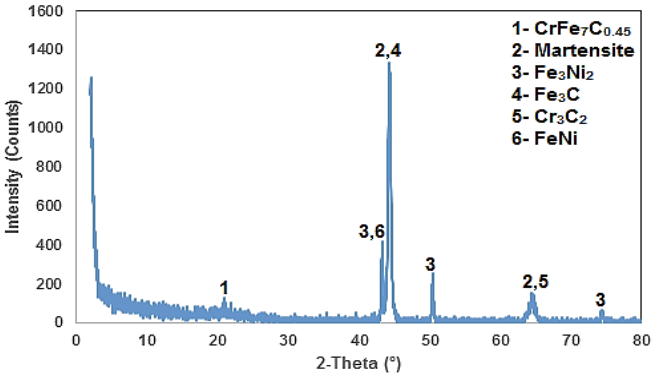

Fig. 3. XRD analysis of S3 joint.

3.3. Impact test

Photograph of the S3 impact test specimen is demonstrated in Fig. 4. Impact strength was determined as S1= 43, S2= 49, S3= 59 (J). The heat input rised with the increase of the welding current. The increase in current intensity widened and deepened the weld pool. Increasing the quantity of δ- ferrite in weld pool reduces the impact toughness. The chromium carbide and sigma phases formed in the welded joint created embrittlement and low impact performance [15]–[17]. Fractured surface SEM image of S1 joint is shown in Fig. 5. Fibrous pits of different sizes and depths and ductile fracture were detected on the fractured surface.

Fig. 4. Impact test image of S3 joint.

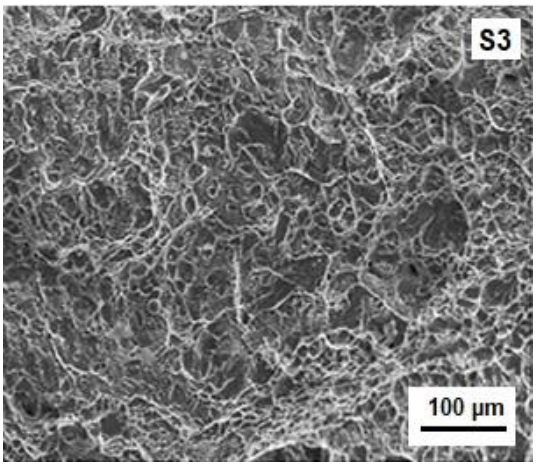

Fig. 5. Fractured surface SEM image of the S1 joint.

IV. CONCLUSION

The thick dissimilar plates were welded using DSAW-TIG welding. The results obtained are summarized below.

Welded joints occurred without any problems.

The steels were joined with full penetration without additional metal and welding gap

The increase in current intensity allowed the weld pool to expand and deepen.

Martensite, Fe_3C, $CrFe_7C_{0.45}$, FeNi, Cr_3C_2 and Fe_3Ni_2 phases were formed in the welded joint.

Impact strength was determined as S1 =43, S2 =49, S3 =59 (J).

ACKNOWLEDGMENT

This study was supported by Adıyaman University Scientific Research Project Unit (Grant number: MUFYL/2019-001).

REFERENCES

[1] M. Yang, C. Li, Y. Zhang, D. Jia, X. Zhang, Y. Hou and J. Wang, ‘‘Maximum undeformed equivalent chip thickness for ductile-brittle transition of zirconia ceramics under different lubrication conditions’’, *Int. J. Mach. Tools Manuf.*, vol. 122, pp. 55–65, 2017.

[2] S. V. Brahimi, S. Yue and K. R. Sriraman, ‘‘Alloy and composition dependence of hydrogen embrittlement susceptibility in high-strength steel fasteners’’, *Philos. Trans. Royal Soc. A.*., vol. 375, pp. 20160407, 2017.

[3] V. E. Panin, L. S. Derevyagina, M. P. Lebedev, A. S. Syromyatnikova, N. S. Surikova, Y. I. Pochivalov and B. B. Ovechkin, ‘‘Scientific basis for cold brittleness of structural BCC steels and their structural degradation at below zero temperatures’’, *Phys. Mesomech*, vol. 20, pp. 125–133, 2017.

[4] V. E. Panin, L. S. Derevyagina, N. M. Lemeshev, A. V. Korznikov, A. V. Panin and M. S Kazachenok, ‘‘On the nature of low-temperature brittleness of BCC steels’’, *Phys. Mesomech*, vol. 17, pp. 89–96, 2014.

[5] K. Guan, Z. Wang, M. Gao, X. Li and X. Zeng, ‘‘Effects of processing parameters on tensile properties of selective laser melted 304 stainless steel’’, *Mater. Des.*, vol. 50, pp. 581–586, 2013.

[6] J. Z. Lu, K. Y. Luo, Y. K. Zhang, G. F. Sun, Y. Y. Gu, J. Z. Zhou, X. D. Ren, X. C. Zhang, L. F. Zhang, K. M. Chen, C. Y. Cui, Y. F. Jiang, A. X. Feng and L. Zhang, ‘‘Grain refinement mechanism of multiple laser shock processing impacts on ANSI 304 stainless steel’’, *Acta Mater.*, vol. 58, pp. 5354–5362, 2010.

[7] M. Aritoshi and K. Okita, ‘‘Friction welding of dissimilar metals’’, *Weld. Int.*, vol. 17, pp. 271–275, 2003.

[8] K. P. Mehta, ‘‘A review on friction-based joining of dissimilar aluminum–steel joints’’, *J. Mater. Res.*, vol. 34, pp. 78–96, 2018.

[9] H. Peng, C. Chen, H. Zhang and X. Ran, ‘‘Recent development of improved clinching process’’, *Int. J. Adv. Manuf. Technol*., vol. 110, pp. 3169–3199, 2020.
[10] S. Cui, Y. Shia, Y. Cui and T. Zhu, ‘‘The impact toughness of novel keyhole TIG welded duplex stainless joints’’, *Eng. Failure Analysis*., vol. 94, pp. 226–231, 2018.
[11] N. Arivazhagan, S. Singh, S. Prakash and G. M. Reddy, ‘‘Investigation on AISI 304 austenitic stainless steel to AISI 4140 low alloy steel dissimilar joints by gas tungsten arc, electron beam and friction welding’’, *Mater. Des*., vol. 32, pp. 3036–3050, 2011.
[12] A. El-Batahgy, A. Saiyah, S. Khafagi, A. Gumenyuk, S. Gook and M. Rethmeier, ‘‘Shielded metal arc welding of 9%Ni steel using matching ferritic filler metal’’, *Sci. Technol. Weld. Join*., vol. 26, pp. 116–122, 2021.
[13] Z. Q. Wang, X. L. Wang, Y. R. Nan, C. J. Shang, X. M. Wang, K. Liu and B. Chen, ‘‘Effect of Ni content on the microstructure and mechanical properties of weld metal with both-side submerged arc welding technique’’, *Mater. Char*., vol. 138, pp. 67–77, 2018.
[14] B. E. Kim, J. Y. Park, J. S. Lee, J. I. Lee and M. H. Kim, ‘‘Effects of the welding process and consumables on the fracture behavior of 9 wt.% nickel steel’’, *Exp. Tech*., vol. 44, pp. 175–186, 2020.
[15] S. Saini and K. Singh, ‘‘Recycling of steel slag as a flux for submerged arc welding and its effects on chemistry and performance of welds’’, *Int. J. Adv. Manuf. Technol*., vol. 114, pp. 1165–1177, 2021.
[16] J. Park, Y. Kim, H. Baek and S. Cho, ‘‘A study on process development of super-TIG welding for 9% nickel steel with Alloy 625’’, *J. Manuf. Process*., vol. 40, pp. 140–148, 2019.
[17] S. Gook, S. Krieger, A. Gumenyuk, A. M. El-Batahgy and M. Rethmeier, ‘‘Notch impact toughness of laser beam welded thick sheets of cryogenic nickel alloyed steel X8Ni9’’, *Procedia CIRP*., vol. 94, pp. 627–631, 2020.